C, 45.81; H, 4.21. Found: C, 45.69; H, 4.17. *trans*-$Cp^*W(CO)_2(PMe_3)Bcat'$ (**4**): ^1H NMR (C_6D_6): δ 6.90 (s, 1H), 6.52 (s, 1H), 2.40 (s, 3H), 2.15 (s, 3H), 1.92 (s, 15H), 1.29 (d, J_{HP} = 8.9 Hz, 9H); ^{13}C {^1H} NMR (C_6D_6): δ 229.63 (d, $^2J_{CP}$ = 19.7 Hz, $^1J_{CW}$ = 143.0 Hz), 152.03, 149.03, 130.43, 123.37, 120.23, 109.96, 102.65, 21.74, 20.35 (d, J_{CP} = 33.0 Hz), 15.42, 11.79; ^{11}B NMR (C_6D_6): δ 58; ^{31}P {^1H} NMR (C_6D_6): δ −10.6 (s, J_{PW} = 273.4 Hz); IR (C_6D_6): ν_{CO} 1906 (m), 1823 (s); analysis calculated for $C_{23}H_{32}BO_4PW$: C, 46.19; H, 5.39. Found: C, 46.30; H, 5.39.

13. H. Nöth and B. Wrackmeyer, in *NMR Basic Principles and Progress*, P. Diehl, E. Fluck, R. Kosfeld, Eds. (Springer-Verlag, New York, 1978), vol. 14, p. 271.
14. The HBcat′ compound was synthesized from BH_3·Me_2S and 3,5-dimethylcatechol in ether.
15. V. Guerchais, C. Lapinte, J.-Y. Thepot, *Organometallics* **7**, 604 (1988).
16. A. Stasunik, D. R. Wilson, W. Malisch, *J. Organomet. Chem.* **270**, C18 (1984).
17. R. J. Kazlauskas and M. S. Wrighton, *J. Am. Chem. Soc.* **104**, 6005 (1982).
18. D. Catheline and D. Astruc, *Organometallics* **3**, 1094 (1984); R. B. King, M. Z. Iqbal, A. D. King, *J. Organomet. Chem.* **171**, 53 (1979); G. O. Nelson and C. E. Sumner, *Organometallics* **5**, 1983 (1986).
19. It is possible that a free boryl radical is reacting with a metal-bound alkane. This mechanism would involve both photochemical dissociation of CO to form a 16-electron complex, which would then bind alkane, and photochemical generation of free boryl radical, which would react with the alkane complex. Although this mechanism is consistent with our data, we suggest two simpler mechanisms.
20. We showed that ^{13}CO was incorporated into the transition metal products, $[Cp^*W(CO)_3]_2$ and $Cp^*W(CO)_3H$, as determined by ^{13}C NMR spectroscopy. However, control reactions showed that ^{13}CO was incorporated into the products under reaction conditions similar to those of the functionalization process.
21. This complex was independently synthesized by reaction of the known $Li[Cp^*W(CO)_2PMe_3]$ [S. Schmitzer *et al.*, *Inorg. Chem.* **32**, 303 (1993)] with ClBcat′. Spectral and analytical data are provided in (*12*).
22. F. A. Cotton and G. Wilkinson, *Advanced Inorganic Chemistry* (Wiley, New York, 1988), vol. 5.
23. P. R. Rablen, J. F. Hartwig, S. P. Nolan, *J. Am. Chem. Soc.* **116**, 4121 (1994).
24. The following references describe alkyl hydride products obtained by C–H activation in related metal complexes: J. K. Hoyano, A. D. McMaster, W. A. G. Graham, *ibid.* **105**, 7190 (1983); A. H. Janowicz and R. G. Bergman, *ibid.*, p. 3929; R. G. Bergman, P. F. Seidler, T. T. Wenzel, *ibid.* **107**, 4358 (1985).
25. M. E. Thompson *et al.*, *ibid.* **109**, 203 (1987).

4 April 1997; accepted 20 May 1997

Element-Specific Magnetic Anisotropy Determined by Transverse Magnetic Circular X-ray Dichroism

H. A. Dürr, G. Y. Guo, G. van der Laan, J. Lee, G. Lauhoff, J. A. C. Bland

Understanding of the magnetocrystalline anisotropy in magnetic materials (the influence of different elemental components on the direction of easy magnetization) can be greatly enhanced by measuring the orbital moment anisotropy of the elemental constituents. A circular x-ray dichroism technique is presented that allows the determination of the microscopic origin of the spin reorientation transition in ultrathin single-crystalline cobalt/nickel films. The stronger anisotropy contribution of a much thinner cobalt layer redirects the easy magnetization direction of the entire film.

Understanding of the magnetic anisotropy in nanostructures is of both scientific and technological importance. In device applications, such as magnetic and magneto-optic recording, the use of different magnetic materials such as alloys or layered systems allows tailoring of the magnetic anisotropy, that is, the easy direction of magnetization. So far it has only been possible to measure the magnetic anisotropy of the total system. We report here the separate measurement of the anisotropy contributions of the elemental constituents with transverse magnetic circular x-ray dichroism (TMCXD). The difference in x-ray absorption between left and right circularly polarized light is measured in a transverse geometry where for an isotropic sample the dichroism signal vanishes.

We studied the changes in the magnetocrystalline anisotropy (MCA) that occurred when an ultrathin Co film was deposited onto a 33-monolayer-(ML)-thick Ni layer. The films were grown and structurally characterized under ultrahigh vacuum conditions as described in detail elsewhere (*1*). The conventional way to obtain information about magnetic anisotropies is through hysteresis loops (Fig. 1). In the 33-ML Ni film, the spins are remanently oriented along the sample normal. Deposition of only 3 ML of Co onto the Ni surface forces the spins into the surface plane. With the magneto-optical Kerr effect, which is the usual method to measure the loops in Fig. 1, it is not possible to distinguish between the different elements Co and Ni (*2*). Magnetometry with conventional MCXD can in principle achieve this by measuring the element-resolved orientation of the spin magnetic moments (*3*). However, because of the strong exchange coupling between Ni and Co, the hysteresis loops for the two elements are identical, making it difficult to differentiate between the different mechanisms describing the behavior displayed in Fig. 1. It has been shown that the perpendicular magnetic anisotropy of the Ni film in Fig. 1 is related to the Ni in-plane lattice expansion in the epitaxial Ni/Cu system (*1*, *4*). Thus, the Co top layer, which favors a smaller lattice parameter than the substrate (*5*), could be forcing the spins in-plane through a strain reduction in the Ni layer. An alternative is that face-centered-cubic Ni and Co lattices respond differently to strain; Ni has an easy magnetization axis perpendicular to the direction of the lattice expansion, whereas the Co spins prefer to be parallel (*6*). We show below the close relation between MCA and the orbital moment anisotropy. Element-specific TMCXD measurements show that it is indeed the stronger in-plane anisotropy of the thinner Co layer that forces the larger magnetic moment of the Ni layer in-plane.

The leading contribution to the MCA is thought to be the spin-orbit coupling (*7*, *8*). It can be shown that, for 3*d* transition metal magnets, the spin-orbit contribution to the ground-state energy E is proportional to the scalar product of the expectation value of the orbital moment vector **L** and a unit vector **S** in the direction of the sample magnetization (*9*)

$$E \propto -\xi \mathbf{L}\cdot\mathbf{S} \qquad (1)$$

where ξ is the spin-orbit coupling parameter. This result is very intuitive. It shows that the spin-orbit coupling tries to align **L** and **S** (anti)parallel to each other to minimize the total energy of the system. The negative sign applies to the transition metals with more than half-filled 3*d* shells and corresponds to a parallel alignment of **L** and **S**. In transition metals, the orbital moment is determined by the interplay of the spin-orbit coupling with the much stronger crystalline field interaction. It is the crystalline field that acts directly on the electron orbits and fixes **L** relative to the crystal lattice. As a consequence, we obtain different values of **L** if the spins are oriented along different crystal directions by a strong external magnetic field. The easy magnetization direction **N** is then given as the direction with the largest component of **L** that results in the lowest energy (Eq. 1). This important relation of the orbital moment and the MCA has recently been verified experimentally by Weller *et al.* (*10*).

L and **S** are parallel when **S** is along a high-symmetry direction of the crystalline

H. A. Dürr, G. Y. Guo, G. van der Laan, Daresbury Laboratory, Warrington WA4 4AD, UK.
J. Lee, G. Lauhoff, J. A. C. Bland, Cavendish Laboratory, University of Cambridge, Cambridge CB3 0HE, UK.

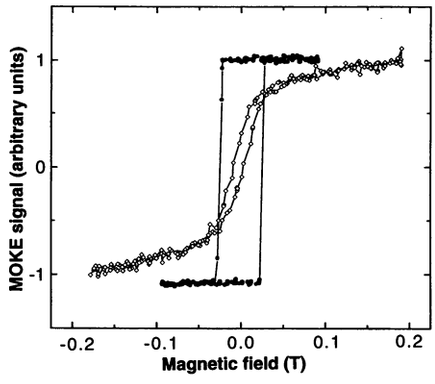

Fig. 1. Hysteresis loops measured with the magneto-optical Kerr effect (MOKE). The magnetic field was applied perpendicular to the sample surface. The MOKE signal is proportional to the sample magnetization along this direction. For the 33-ML Ni film (lines and solid symbols), a rectangular loop shows that the Ni spins align remanently along the surface normal. Co deposition causes a spin reorientation into the surface plane. For 3-ML Co on a 33-ML Ni film (lines and open symbols), the hysteresis loop shows mainly in-plane magnetization. The reduced remanence at zero magnetic field indicates that there is still a small perpendicular magnetization component. At higher Co thicknesses, all of the Co and Ni spins are completely in-plane. The Co and Ni films were evaporated onto a 550-ML Cu/Si(100) substrate and capped with a 15-ML-thick Cu layer to prevent oxidation (*1*).

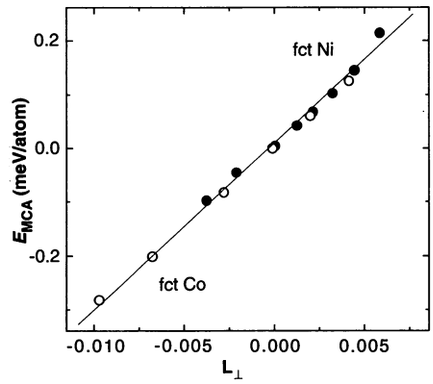

Fig. 3. Relation between the transverse orbital moment $\mathbf{L}_\perp$ (in units of $\hbar = 1$) and the magnetocrystalline anisotropy energy E_{MCA}, which is the energy difference between spin alignment perpendicular and parallel to the film plane. $\mathbf{L}_\perp$ can be shown to be half the difference in **L** with the spins aligned perpendicular and parallel to the film plane (*9*) and was calculated in this way. Calculations were performed for face-centered tetragonal (fct) Co and Ni lattices with distortions of up to ±3.3%. The drawn line is a linear fit to the data.

structure. If the spins are forced to align along a nonsymmetry crystal direction by an external magnetic field, a situation arises as depicted in the insets of Fig. 2. The broken symmetry no longer restricts **L** and **S** to be parallel. Spin-orbit interaction still tries to align **L** parallel to **S**. This is partially counteracted by the crystalline field, which pulls **L** towards **N**, thus causing a component of **L** perpendicular to **S**. The size of $\mathbf{L}_\perp$ is a measure of the MCA, the strength to restore the spin alignment along **N**. $\mathbf{L}_\perp$ can be shown to be proportional to E_{MCA}, which is defined as the energy difference between spin alignment perpendicular and parallel to the film surface (*9*, *11*).

The orbital moment can ideally be studied with MCXD. Sum rules relate the integrated x-ray absorption signals at the $L_{2,3}$ edges for left and right circularly polarized x-rays to ground-state magnetic properties, such as the orbital moment and the number of 3*d* holes n_h (*12*). Circularly polarized light is characterized by a helicity vector **P** along the propagation direction. The projection of **L** onto **P** can be obtained from (*12*)

$$\mathbf{L}\cdot\mathbf{P} = -n_h \frac{4}{3}\frac{\Delta A}{A} \qquad (2)$$

where A and ΔA are the integrated areas for the sum and difference spectra of the two light helicities, respectively. The measurement for the 33-ML Ni film is shown in Fig. 2A. The data were obtained on beamline 1.1 of the Synchrotron Radiation Source Daresbury with 80% circularly polarized x-rays. A 2-T magnetic field from a superconducting magnet was used to saturate the sample. The field was reversed while the light helicity was kept fixed, which results in the two spectra at the top in Fig. 2A; the difference signal is displayed at the bottom. We chose a geometry where the magnetic field **H**, and consequently **S**‖**H**, was perpendicular to **P**. The x-rays were incident at an angle of 45° relative to the surface. According to Eq. 2, we then measured $\mathbf{L}_\perp$. The obtained value is $\mathbf{L}_\perp/n_h = -0.010 \pm 0.005$ (in units of $\hbar = 1$, where $\hbar$ is Planck's constant divided by 2π). The sign of $\mathbf{L}_\perp$ determines the direction of **L** and demonstrates that **N** is along the sample normal (compare with the inset to Fig. 2A). A similar measurement at the Ni $L_{2,3}$ edges of the 3-ML Co/33-ML Ni film gave an identical result, which shows that, for this sample, the Ni spins also prefer to be perpendicular to the film plane. The in-plane magnetization for the total Co/Ni system must be due to the Co orbital anisotropy; measurements at the Co $L_{2,3}$ edges (Fig. 2B) show that the Co TMCXD spectrum has the opposite sign as compared with that of Ni and show its tendency to order in-plane. We obtain a value

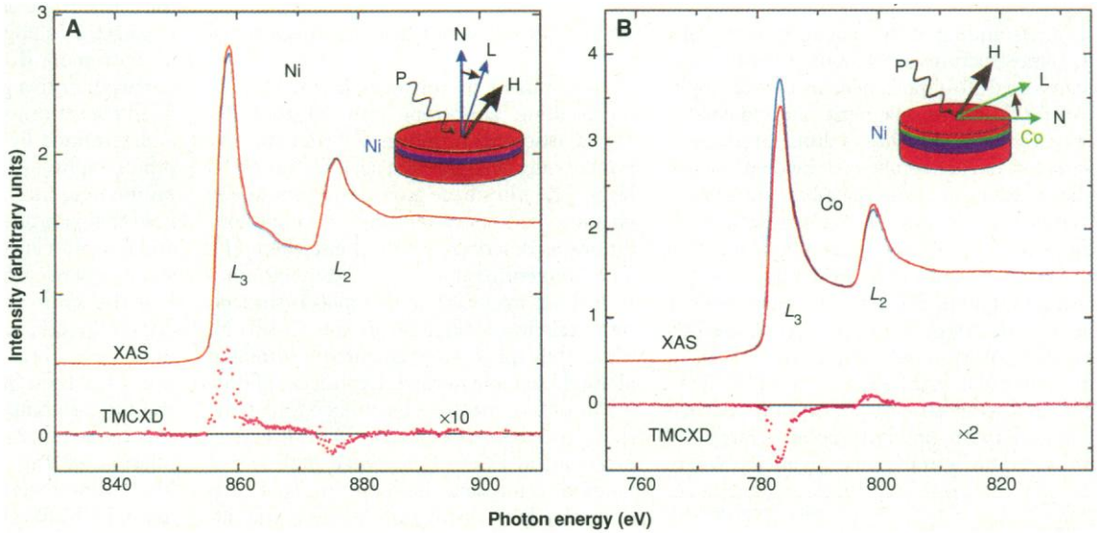

Fig. 2. X-ray absorption spectra (XAS) taken in the total yield detection mode with 80% circularly polarized light (**A**) at the Ni $L_{2,3}$ edges of 33-ML Ni and (**B**) at the Co $L_{2,3}$ edges of 3-ML Co/33-ML Ni films. The upper traces in both figures show the effect of a reversal of the magnetic field **H** on the XAS spectra (blue and red lines). The TMCXD spectrum (symbols) is the difference of the XAS spectra obtained for the two magnetization directions. Diagrams in upper right corners show schematic views of the measurement geometry depicting the relative orientation of magnetic field, light helicity vector **P**, and orbital magnetic moment vector **L**; the vector **N** gives the easy direction of magnetization.

of $\mathbf{L}_\perp/n_h = 0.050 \pm 0.005$, which is thus five times larger than that of Ni.

For a direct comparison of the E_{MCA} in Ni and Co, we need to know the proportionality factors in Eq. 1. We performed fully relativistic first-principles band structure calculations in the local spin-density approximation (*13*) for both Co and Ni (Fig. 3). Their face-centered lattices were tetragonally distorted to various degrees, resulting in a simultaneous change in E_{MCA} and $\mathbf{L}_\perp$. These quantities show a linear relation with the same proportionality factor over a wide distortion range. This is surprising, because ξ for Ni is about 12% greater than that for Co. The small deviations from the linear behavior can be assigned to additional terms neglected in Eq. 1, such as the magnetic dipole contribution (9). Applying the curve in Fig. 3 to our experimental data, we obtain for the magnetic anisotropy energy of the 33-ML Ni and 3-ML Co layers per unit cell values of $E_{MCA}^{Ni} = 14$ meV and $E_{MCA}^{Co} = -11$ meV (*14*), where we used the calculated number of 3*d* holes of $n_h^{Ni} = 1.4$ and $n_h^{Co} = 2.4$. The measurements show unambiguously that the Ni spins in both cases favor a perpendicular orientation, and it is the anisotropy contribution of the Co layer that determines the spin orientation of the entire film. For the 3-ML Co/33-ML Ni film, the anisotropy contributions nearly cancel each other, resulting in the mixed in-plane and perpendicular easy-axis characteristics of Fig. 1. A small increase in the Co layer thickness causes a negative total anisotropy energy, and consequently, the easy magnetization direction will be completely in the film plane in agreement with the hysteresis measurements.

The strong exchange interaction through the Co/Ni interface mediated by 3*d* electrons couples the spins of the two layers parallel (*2*). Our element-specific TMCXD measurements establish the competition between the in-plane anisotropy of the Co orbital moment and the out-of-plane anisotropy of the Ni layer. This leads to the observed Co thickness-dependent reorientation of the total spin magnetic moment. Such measurements can be performed in a fixed geometry and only involve monitoring of the x-ray absorption cross-section, which in principle can be done in reflection or transmission. Combined with x-ray microscopy, this technique could be used to image magnetic anisotropy of nanostructures and devices.

REFERENCES AND NOTES

1. J. Lee, G. Lauhoff, J. A. C. Bland, *Europhys. Lett.* **35**, 463 (1996).
2. M. T. Johnson *et al.*, *Phys. Rev. Lett.* **69**, 3575 (1992).
3. V. Chakarian *et al.*, *Phys. Rev. B* **53**, 11313 (1996).
4. C. A. Chang, *J. Appl. Phys.* **68**, 4873 (1990).
5. J. Fassbender *et al.*, *Phys. Rev. Lett.* **75**, 4476 (1995).
6. Landolt-Bornstein New Series, vol. 19a, H. P. J. Wijn, Ed. (Springer-Verlag, Berlin, 1986).
7. P. Bruno, *Phys. Rev. B* **39**, 865 (1989).
8. M. Cinal, D. M. Edwards, J. Mathon, *ibid.* **50**, 3754 (1994).
9. H. A. Dürr and G. van der Laan, *ibid.* **54**, R760 (1996).
10. D. Weller *et al.*, *Phys. Rev. Lett.* **75**, 3752 (1995); H. A. Dürr, G. van der Laan, B. T. Thole, *ibid.* **76**, 3464 (1996).
11. MCA is usually described as a perturbation expansion in ξ (*8*). In low-symmetry nanostructures, the dominant contribution is the so called uniaxial anisotropy, which is of second order in ξ. Only this term is considered here.
12. B. T. Thole, P. Carra, F. Sette, G. van der Laan, *Phys. Rev. Lett.* **68**, 1943 (1992).
13. G. Y. Guo, W. M. Temmerman, H. Ebert, *Physica B* **172**, 61 (1991).
14. Using the Cu substrate unit cell of 0.255 by 0.255 nm, we obtain $E_{MCA}^{Ni} = 34$ mJ/m^2 and $E_{MCA}^{Co} = -27$ mJ/m^2. These values come out to be very large (*2*), probably because band structure calculations overestimate the proportionality factor between E_{MCA} and $\mathbf{L}_\perp$ (*10*).

14 March 1997; accepted 21 May 1997

Glacial Cycles and Astronomical Forcing

Richard A. Muller and Gordon J. MacDonald

Narrow spectral features in ocean sediment records offer strong evidence that the cycles of glaciation were driven by astronomical forces. Two million years ago, the cycles match the 41,000-year period of Earth's obliquity. This supports the Croll/Milankovitch theory, which attributes the cycles to variations in insolation. But for the past million years, the spectrum is dominated by a single 100,000-year feature and is a poor match to the predictions of insolation models. The spectrum can be accounted for by a theory that derives the cycles of glaciation from variations in the inclination of Earth's orbital plane.

Nearly as soon as the ice ages were discovered, their origin was attributed to astronomical causes. In the late 1800s, James Croll assumed that the ice ages were driven by changes in insolation (solar heating) brought about by variations in Earth's orbit and spin axis (*1*, *2*). According to Croll, and to Milankovitch after him (*3*, *4*), the main orbital parameters that affect insolation and its distribution are Earth's orbital eccentricity, obliquity (the tilt of Earth's poles toward the sun), and precession (the lag between equinox and perihelion). However, it was not until 1970 that Broecker and van Donk (*5*) established that glaciation in the late Pleistocene was truly periodic and was dominated by a 100,000-year (100-ky) cycle. This period was soon identified with the quasiperiodic 100-ky cycle of Earth's eccentricity. (We will offer evidence that this identification was premature.) In addition, another strong cycle was discovered with a 41-ky period that matched the cycle of changes in Earth's obliquity (*6*). This 41-ky cycle appears to have dominated glacial changes from 1.5 to 2.5 million years ago (Ma) (*7*). The 100-ky cycle has dominated from 1 Ma to the present.

Much of the best data for paleoclimate studies comes from ocean sediments, in which proxies for climate, preserved in fossils, are measured as a function of depth. The oxygen isotope ratio $\delta^{18}O$ is believed to reflect the amount of Earth's water frozen in ice and thus is a measure of Earth's global ice volume. To turn a record of $\delta^{18}O$ versus depth into a record versus time, the sedimentation rate must be estimated. This is often done with a process called tuning, in which the instantaneous sedimentation rate is deduced by matching cycles in $\delta^{18}O$ to calculated perturbations in Earth's orbit. Parameterized sedimentation rates are adjusted to bring the observed proxy variations into consonance with the predictions of the model. This approach is potentially circular if the results are used to validate the climate model used to tune the record. Neeman (*8*) has demonstrated with Monte Carlo tests that, given enough parameters, tuning procedures can successfully match data to an incorrect model, resulting in an inaccurate time scale as well as in a false validation of the model. Therefore, for the present work, we emphasize the use of time scales that are untuned and assume constant sedimentation with average rates constrained by radiometrically measured control points.

A strong case for astronomical forcing of glacial cycles comes from analysis of $\delta^{18}O$ data for the age interval 1.5 to 2.5 Ma from Deep Sea Drilling Project (DSDP) site 607, located on the west flank of the Mid-Atlantic Ridge. For a full description of the stratigraphy, dating, and magnetic correlation, see Ruddiman *et al.*

R. A. Muller, Department of Physics and Lawrence Berkeley Laboratory, University of California, Berkeley, CA 94720, USA.
G. J. MacDonald, International Institute for Applied Systems Analysis, A-2361 Laxenburg, Austria.